Proceedings of the ASME 2009 28th International Conference on Ocean, Offshore and Arctic Engineering
OMAE2009
May 31 - June 5, 2009, Honolulu, Hawaii, USA

OMAE2009-79468

ON THE COUPLED EXTENSIONAL–TORSIONAL RESPONSE OF FLEXIBLE PIPES

Héctor E. M. Merino
LABEST/COPPE/UFRJ
Rio de Janeiro, Brazil

José R. M. de Sousa
LACEO/COPPE/UFRJ
Rio de Janeiro, Brazil

Carlos Magluta
LABEST/COPPE/UFRJ
Rio de Janeiro, Brazil

Ney Roitman
LABEST/COPPE/UFRJ
Rio de Janeiro, Brazil

ABSTRACT

In this paper, the coupled extensional-torsional behavior of a 4" flexible pipe is studied. The pipe was subjected to pure tension and two different boundary conditions were considered: ends free and prevented from axially rotating. The response of the pipe is predicted with a three-dimensional nonlinear finite element (FE) model. Some aspects of the obtained results are discussed, such as: the effect of restraining the axial rotation at the extreme sections of the model; the effect of friction or adhesion between the layers of the pipe on the induced axial rotation (or torque) and elongation; and the reduction to simple plane behavior usually assumed by analytical models. The numerical results are compared to the ones measured in experimental tests performed at COPPE/UFRJ. Reasonable agreement is observed between all results pointing out that the analyzed pipe is torque balanced and that friction mainly affects the axial twist or torque led by the applied tension. Moreover, the cross-sections of the pipe remain straight with the imposed load, but different axial rotations are found in each layer.

INTRODUCTION

Flexible risers (Fig. 1) are key components in the design and successful operation of floating facilities devoted to drill, produce, store or off-load offshore oil and gas. They are composite pipes made up of several concentric polymeric and metallic layers which, working together, provide flexibility as well as high axial and pressure resistance. The polymeric layers work as sealing and/or anti-wear components, while the metallic layers withstand the imposed loads. There are basically three different types of metallic layers: There are basically three different types of metallic layers:

1. *Inner carcass*: made from profiled steel strips wounded at angles close to 90° (see Fig. 1), which mainly resists to radial inward forces.
2. *Pressure armor*: usually made from Z-shaped steel wires wounded at angles close to 90° (see Fig. 1), which supports the system internal pressure and also radial inward forces.
3. *Tensile armors*: these layers typically use rectangular (most common) or round shaped steel wires laid in two or four layers and cross-wounded at angles between 30° and 55°. They resist to tension, torque and pressure end cap effects.

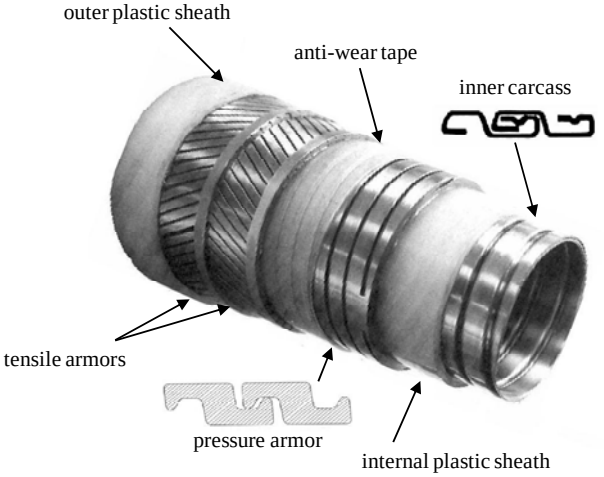

Figure 1 – Typical flexible pipe.

The problem of evaluating the local structural response of these structures has been dealt in the literature with analytical and numerical models and also experimental tests. Most of them are devoted to predict their response to moderate axisymmetric or bend loads.

On the analytical side, Ferét and Bournazel [1] formulated a set of linear equations that governs the response of flexible

pipes made of long concentric tubular and helicoidal armor layers. Witz and Tan [2] proposed an analytical nonlinear model that predicts the axial-torsional structural behavior of flexible risers. The model considers that the polymeric layers are long thin-walled cylinders and the behavior of the helical armors is governed by Love's equilibrium equations for thin helical rods. Separation between layers is also addressed. Recently, Custódio and Vaz [3] and Saevik and Bruaseth [4] proposed analytical models which aggregated some improvement to the available ones by considering geometric, material and contact nonlinearities in the analysis of slender tubular structures such as umbilical cables and flexible risers. These authors also presented detailed experimental results from axisymmetric tests with umbilical cables.

On the numerical side, Ribeiro *et al.* [5], based on the previous works of Cruz [6] and Sousa [7] presented a three-dimensional finite element model to study the response of flexible risers under pure tension or axial compression. The model consisted of a "sandwich" of concentric thin shells, which represented the inner carcass, the pressure armor and all polymeric layers. The wires of the tensile armor were modeled with three-dimensional beam elements. Interaction between layers was established with non-linear springs. Recently, Bahtui *et al.* [8] studied the response of a five-layer (three polymeric layers and a pair of tensile armor layers) flexible pipe to pure tension with a detailed three-dimensional finite element model. In this model, sheath layers are represented with three-dimensional eight-noded solid elements. Contact elements are defined between each layer and no interaction is considered between tendons of helical armor layers. Moreover, friction between layers are addressed. According to the authors, very good agreement between the proposed model and analytical ones was found, but the model demanded great computational effort. Besides, the presented analyses did not consider the presence of the inner carcass and/or the pressure armor which would probably lead to an even more complex and onerous model.

Furthermore, there are two experimental works which is worth to mention: the one from Witz [9] and, recently, the study presented by Ramos Jr. *et al.* [10]. Witz [9] carried out an interesting study in which the axial and torsional stiffness of a 2.5" flexible pipe were experimentally evaluated considering different boundary conditions at the extremities of the pipe. The bending stiffness was also experimentally estimated with different levels of internal pressure. The author detailed described the internal layers of the pipe and proposed a "blind" test to several institutions by asking them to estimate those stiffness with their models. Generally, the results provided by the models agreed well with the experimental ones for the extensional-torsional response of the pipe. Bending results were, however, considerably more scattered. Witz [9] assigns that the key feature to correctly predict the local structural behavior of a flexible pipe is to account for the interaction between all its layers. Moreover, a study considering combined tension, torsion, pressure and bend loads were suggested as well as more tests to confirm the presented experimental results.

Ramos Jr. *et al.* [10] recently presented a set of experimental tests with a 2.5" flexible pipe in order to study its extensional-torsional response. The pipe was subjected to tension with and without internal pressure and with different boundary conditions at its ends. Detailed information about the internal structure of the flexible pipe is presented and the experimental results were compared to the ones from a previously stated model (Ramos Jr. and Pesce [11]). The authors point that the analytical model predicted well the axial stiffness of the pipe and the average strains in the outer tensile armor wires. However, the measured torque or twist in the pipe due to the applied tension had a highly nonlinear behavior and, therefore, the analytical model failed to predict these values. Part of the differences between the results was attributed to the inability of the analytical model to address the structure internal friction. Furthermore, the studied structure was torque-balanced and the applied internal pressure did not affect its axial stiffness.

Hence, despite their computational efficiency, analytical models assume in a certain extent a set of simplifying assumptions that may interfere in the overall response of the flexible pipe and, according to Custódio and Vaz [3], can be divided in four groups:

1. Regularity of initial geometry.
2. Reduction to simple plane cross-section analysis.
3. Neglection of the effects of shear and internal friction.
4. Linearity of the response.

Thus, in this work, a three-dimensional nonlinear finite element (FE) model capable of simultaneously modeling the flexible riser and different types of mechanical loads is presented. This FE model accounts for all layers of the riser as well as possible interactions between them. Geometric, material and contact nonlinearities, including friction, are also addressed. Therefore, from the four major groups of assumptions, the proposed model will keep only the first one. In order to validate this model, a set of experimental tests is presented. In these tests, performed at COPPE/UFRJ, a 4,0" flexible pipe is subjected to pure tension. The effect of having the axial rotation at the ends of the pipe restrained or not is evaluated. The measured axial rotations, elongations and external radial displacements are compared to the values predicted by the numerical model. Furthermore, the effect of internal friction and the commonly assumed hypothesis of simple plane behavior are also discussed.

FE MODEL

General remarks

Figure 2 presents a general overview of the developed model.

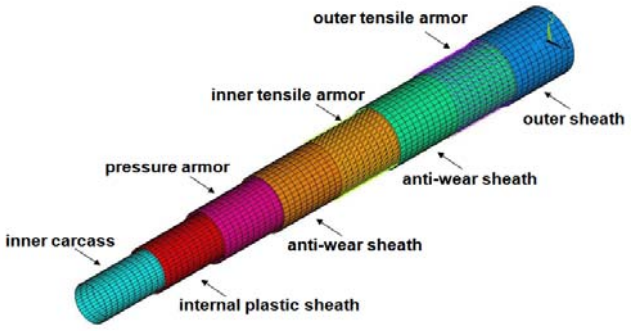

Figure 2 – Isometric view of the numerical model.

The model consists of various concentric thin-walled shells, which represent each layer of the pipe except the wires of the tensile armors which are modeled with three-dimensional beam elements. Interaction between layers is assured through the presence of contact elements. The whole model is detailed hereafter.

Inner carcass and pressure armor representation

The construction of a solid three-dimensional finite element model to direct represent the inner carcass and the pressure armor of flexible risers is, by itself, an extremely onerous computational task (Bahtui *et al.* [8]), due to the high number of degrees of freedom involved. Thus, an alternative approach capable of reducing the number of degrees of freedom and, at the same time, adequately modeling these layers is necessary.

Firstly, it is reasonable to suppose that:

1. The internal friction in these layers is negligible.
2. There is no interaction between the laying direction of the tendons and their normal direction.

In this work, the term tendon refers to the profiled steel strip that forms the inner carcass and also to each wire that constitute the pressure armor. These hypotheses are acceptable as the tendons that constitute these layers are laid in angles close to 90° and the interlocking process leaves internal gaps. Hence, these layers could be considered as helical beams and modeled, for instance, with three-dimensional beam elements. However, these tendons have very small pitch and, consequently, a large number of beam elements is necessary and the computational cost of the model would be also high.

Hobbs and Raoof [12] and Raoof and Hobbs [13] dealt with the problem of calculating the mechanical properties of strands and wire ropes by representing the various layers of helical wires with equivalent orthotropic shells. Relying on this approach, several different problems related to the static and dynamic response of wire ropes were successfully studied (see Kraincanic [14]). Thus, in this work, an analogy between helical tendons and orthotropic shells is also established, but considering a finite element approach. The main idea is to assure that both structures (helical tendon and orthotropic shell) have the same stiffness and extreme (inner and outer) fiber stresses.

Analogy between helical tendons and orthotropic shells

Initially, more two hypotheses are assumed:

3. The thicknesses of the inner carcass and of the pressure armor are small in comparison to the internal diameter of the layer.
4. Shear effects are negligible meaning that the linear elements perpendicular to the middle plane of the structure remain straight and normal to the deflection surface of the structure after bending.

Considering hypotheses 1 to 4, the inner carcass and the pressure armor can be seen as orthotropic shells. Hence, considering the coordinated axes pointed out in Fig. 3, the stress-strain relations are given in Eq. (1).

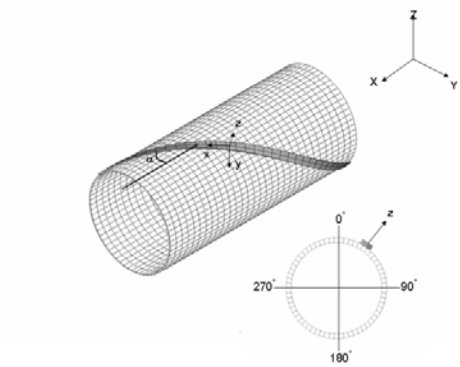

Figure 3 – Coordinate systems.

$$\begin{cases} \sigma_{s_x} = \dfrac{E_{s_x}}{1-\nu_{s_{xy}}\cdot\nu_{s_{yx}}}\cdot\varepsilon_{s_x} + \dfrac{E_{s_x}\cdot\nu_{s_{yx}}}{1-\nu_{s_{xy}}\cdot\nu_{s_{yx}}}\cdot\varepsilon_{s_y} \\ \sigma_{s_y} = \dfrac{E_{s_y}\cdot\nu_{s_{xy}}}{1-\nu_{s_{xy}}\cdot\nu_{s_{yx}}}\cdot\varepsilon_{s_x} + \dfrac{E_{s_y}}{1-\nu_{s_{xy}}\cdot\nu_{s_{yx}}}\cdot\varepsilon_{s_y} \\ \tau_{s_{xy}} = G_{s_{xy}}\cdot\gamma_{s_{xy}} \end{cases} \quad (1)$$

where σ_s and τ_s are, respectively, the normal and shear stresses at the shell surface; ε_s and γ_s are, respectively, its elongation and angular distortion; E_s, G_s and ν_s are, in this order, the Young modulus, the shear modulus and the Poisson coefficient of the material that constitutes the shell; and subscripts x and y designate the direction to which the mentioned values are related.

As, by hypotheses 1 and 2, the tendons of the inner carcass and the pressure armor do not resist to loads normal to their laying direction, it can be assumed that $E_{s_y} = 0$ and $\nu_{s_{yx}} = \nu_{s_{xy}} = 0$. Therefore, Eq. (1) reads:

$$\sigma_{s_x} = E_{s_x}\cdot\varepsilon_{s_x},\ \sigma_{s_y} = 0,\ \tau_{s_{xy}} = G_{s_{xy}}\cdot\gamma_{s_{xy}} \quad (2)$$

Considering Eq. (2), the stiffness of the equivalent orthotropic shell according to Timoshenko and Woinowsky-Krieger [15] are given by:

$$(EA)_s = h_s \cdot E_{s_x} \ , \ (EI)_s = \left(\frac{h_s^3}{12}\right) \cdot E \ , \ (GJ)_s = \left(\frac{h_s^3}{3}\right) \cdot G_{s_{xy}} \qquad (3)$$

where $(EA)_s$, $(EI)_s$ and $(GJ)_s$ are, respectively, the membrane, bending and torsional stiffness of the orthotropic shell; and h_s is its thickness.

The stiffness of an helical tendon, according to Timoshenko and Woinowsky-Krieger [15] are expressed as:

$$(EA)_t = \left(\frac{A \cdot n_t}{L_p}\right) \cdot E \ , (EI)_t = \left(\frac{I_{eq} \cdot n_t}{L_p}\right) \cdot E \ , (GJ)_t = \left(\frac{J \cdot n_t}{L_p}\right) \cdot G \qquad (4)$$

where $(EA)_t$, $(EI)_t$ and $(GJ)_t$ are the axial, bending and torsional stiffness of the tendon; E and G are the Young and shear modulus of the material that constitute the tendon; n_t is the number of tendons in the considered layer, which is, generally, 1 for the inner carcass and 1 or 2 for the pressure armor; A and J are the cross-sectional area and the torsional constant of the tendon; L_p is the pitch of the tendon:

$$L_p = \frac{2 \cdot \pi \cdot R}{\tan(\alpha)} \qquad (5)$$

where R is the mean radius of the layer and α is the lay angle of the tendon.

Recently, Souza [16], based on a series of experimental tests, proposed that the equivalent moment of inertia of the wire, I_{eq}, is given by:

$$I_{eq} = 12 \cdot n_t \cdot \frac{I_y^2}{L_p} \cdot \frac{1-\nu^2}{h^3} \qquad (6)$$

where ν is the Poisson coefficient of the material that constitute the tendon and h is its height; I_y is the lower moment of inertia of the tendon cross-section.

Equaling Eqs. (3) and (4) and considering Eq. (6), the equivalent physical and geometric properties of the orthotropic shell are:

$$h_s = \sqrt{12 \cdot \frac{I_{eq}}{A}} \ , \ E_{s_x} = \left(\frac{n_t \cdot A}{L_p \cdot h_s}\right) \cdot E \ , \ G_{s_{xy}} = \left(\frac{3 \cdot n_t \cdot J}{L_p \cdot h_s^3}\right) \cdot G \qquad (7)$$

At this point, the stress-strain relations of the orthotropic shell are defined in Eqs. (2) and (7). Thus, the stiffness of the helical tendons and of the orthotropic shells can be made equal. Nevertheless, the equivalence between the stiffness of the helical tendon and the orthotropic shell does not imply the equivalence between stresses. According to Timoshenko and Woinowsky-Krieger [15], the extreme (outer and inner) fiber stresses at the orthotropic shell are:

$$\sigma_{s_x}^m = \frac{N_x}{h_s} \ , \ \sigma_{s_x}^b = \frac{6 \cdot M_y}{h_s^2} \ , \ \tau_{s_{xy}} = \frac{6 \cdot M_{xy}}{h_s^2} \qquad (8)$$

where $\sigma_{s_x}^m$, $\sigma_{s_x}^b$ and $\tau_{s_{xy}}$ are, respectively, the membrane, bending and shear stress at the extreme fibers of the orthotropic shell; N_x is the normal force acting in direction x; M_y is the bending moment in y; and M_{xy} is the torsional moment.

The stresses at the extreme fibers of the helical tendon, according to Timoshenko and Woinowski-Krieger [15], can be stated as:

$$\sigma_{t_x}^n = \frac{L_p \cdot N_x}{n_t \cdot A} \ , \ \sigma_{t_x}^b = \frac{L_p \cdot h \cdot M_y}{2 \cdot n_t \cdot I_{eq}} \ , \ \tau_{t_{xy}} = \frac{L_p \cdot t \cdot M_{xy}}{n_t \cdot J} \qquad (9)$$

where $\sigma_{t_x}^n$, $\sigma_{t_x}^b$ and $\tau_{t_{xy}}$ are the normal, bending and shear stress at the extreme fibers of the tendons; t is the thickness of the metallic strip or of the wire that form the tendons of the inner carcass or the pressure armor.

Dividing each related stress in Eqs. (8) and (9), the relations between the extreme fiber stresses of the helical tendon and the equivalent orthotropic shell can be deduced. These relations are called stress correction factors and are given by:

$$f_{c_m}^\sigma = \frac{L_p \cdot h_s}{n_t \cdot A} \ , \ f_{c_b}^\sigma = \frac{L_p \cdot h}{n_t \cdot A} \ , \ f_{c_s}^\sigma = \frac{L_p \cdot t}{n_t \cdot J} \cdot \frac{h_s^2}{6} \qquad (10)$$

where $f_{c_m}^\sigma$, $f_{c_b}^\sigma$ and $f_{c_s}^\sigma$ are the membrane, bending and shear stress correction factors.

Once the stresses are calculated with the proposed model, the extreme fiber stresses in the tendons of the inner carcass or of the pressure armor (σ_{t_x} and $\tau_{t_{xy}}$) are:

$$\sigma_{t_x} = f_{c_m}^\sigma \cdot \sigma_{s_x}^m \pm f_{c_b}^\sigma \cdot \sigma_{s_x}^b \ , \ \tau_{t_{xy}} = f_{c_s}^\sigma \cdot \tau_{s_{xy}} \qquad (11)$$

where the signs ± refers to the outer or inner fibers of the tendon.

It is also possible, by re-writing Eqs. (8) and (9) in terms of strains, to establish strain correction factors:

$$f_{c_m}^\varepsilon = 1 \ , \ f_{c_b}^\varepsilon = \frac{h}{h_s} \ , \ f_{c_s}^\varepsilon = \frac{1}{2} \cdot \frac{t}{h_s} \qquad (12)$$

where $f_{c_m}^{\varepsilon}$, $f_{c_b}^{\varepsilon}$ and $f_{c_s}^{\varepsilon}$ are the membrane, bending and shear strain correction factors.

The strains at the extreme fibers of the tendons can be calculated with Eq. (11) by substituting the stresses for the related strains.

Polymeric layers representation

The inner liner, the anti-wear layers and the outer sheath of flexible risers are modeled as thin-walled cylinders with physical properties equal in all directions, *i. e.*, they are represented by isotropic shell elements. Some flexible risers, however, also have polymeric bandages to prevent the failure by excessive axial compression. These bandages are wounded at angles close to 90° and, consequently, are modeled as orthotropic shells and resist only to tension, which introduces a non-linear physical behavior.

Tensile armor representation

Each helical wire of the tensile armors is modeled with three-dimensional beam elements. As the width and the thickness of these wires are usually much smaller than their length, they could be considered as slender structures and, consequently, shear effects are neglected and Euler-Bernoulli elements are employed.

The wires are normally rectangular shaped and assumed to be perfectly conformed to the cylinder that supports them. Hence, the wire cross-section principal inertia axis is aligned with a vector that links the center of the riser's cross-section to the center of the wire's cross-section.

Modeling contact nonlinearities

In the proposed model, the interaction between the layers of the flexible riser is established with surface to surface contact elements. These elements allow large relative displacement between the layers by using a contact detection algorithm based on the pinball technique (see Belytschko and Neal [17]) and contact forces evaluated with the augmented Lagrangian method (see Belytschko *et al*. [18]).

The augmented Lagrangian method consists of calculating a series of penalty forces during the equilibrium iterations so that the final penetration between the two contact bodies is smaller than a value previously established. In the developed model, an allowable penetration of 0.1% of the smaller thickness between the two layers in contact is adopted.

Penalty forces are calculated by placing fictitious springs along the contact boundaries of two bodies. When contact is established, these forces are applied to the nodal points of the contact elements placed along the contact bodies. The forces are proportional to the penetration and a chosen penalty parameter, which can be physically interpreted as the stiffness of the springs. The choice of this stiffness, called normal contact stiffness, may be performed with relatively simplicity, but respecting some rules. On the one hand, very high values may lead to numerical instabilities and, on the other hand, very small values provoke violations of the contact conditions. Different estimates of contact normal stiffness proposed in Belytschko and Neal [17] and Benson and Hallquist [19], for instance, points to a value equivalent to the stiffness of the elements in contact.

As an estimate of the normal contact stiffness, suppose two cylindrical layers of a flexible riser in contact due to the action of a distributed load, as shown in Fig. 4a.

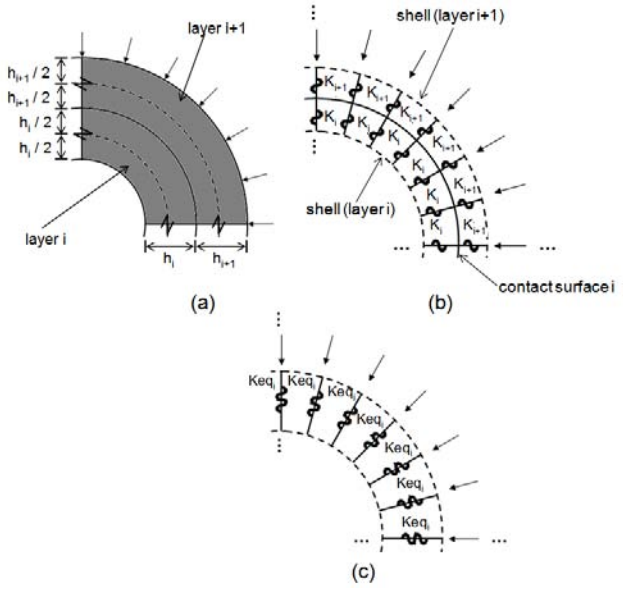

Figure 4 – Schematic representation of the normal stiffness of contact elements.

Now, an equivalent model is idealized by substituting the solid layers by shells connected by two springs in series, each one having the stiffness equivalent to half the thickness of the considered solid layer, as presented in Fig. 4b. The stiffness of each spring, *K*, for a given layer *i*, is:

$$K_i = 2 \cdot \frac{E_i \cdot A_{c_i}}{h_i} \tag{13}$$

where A_c is the contact area, which is approximated by:

$$A_{c_i} = \frac{2 \cdot \pi \cdot \left(R_{c_i} - \frac{h_{c_i}}{2} \right)}{n_{cd_i}} \cdot \frac{L}{n_{ld_i}}, \; i = 1 \ldots n_l - 1 \tag{14}$$

where R_c, h_c, n_{cd} and n_{ld} are, in this order, the mean radius, the thickness, the number of circumferential divisions and the number of longitudinal divisions of the inner layer upon which the contact elements are placed; and n_l is the number of layers in the flexible riser.

The normal contact stiffness, K_{eq}, for the contact elements of the interface *i* is (Fig. 4c):

$$K_{eq_i} = \frac{K_i \cdot K_{i+1}}{K_i + K_{i+1}},\ i = 1...n_l - 1 \qquad (15)$$

Friction between layers is addressed by considering the Coulomb friction model. The presence of gaps between layers is directly accounted in the FE mesh by assuming that the mean radius of a given layer is equal to its original radius plus the gap dimension.

Modeling material nonlinearities

Nonlinear material behaviour is assessed by the sub-layer model or Besseling model (see Besseling [20]) and the relation between uniaxial stress state from tensile tests and multiaxial stress state is established with the yield criterion from Von Mises considering associative flow rule. The stress-strain relationship of each material that constitutes the flexible riser is approximated by the Ramberg-Osgood curve:

$$\varepsilon(\sigma) = \frac{\sigma}{E} \cdot \left[1 + c_1 \cdot \left(\frac{\sigma}{\sigma_y} \right)^{c_2} \right] \qquad (16)$$

where σ_y is the yield stress of the material; and c_1 and c_2 are Ramberg-Osgood constants.

This curve can be directly applied to represent the stress-strain relation of the tensile armors wires and polymeric layers. For the inner carcass and the pressure armor, the FE stresses have to be corrected by the factors presented in Eq. (10). As it will be pointed in the next section, the FE model was implemented using a commercial finite element package (ANSYS®) which allows the creation of user subroutines in Fortran 90 that are applied during the solution procedure. Therefore, a subroutine to automatically correct the stresses in the inner carcass and the pressure armor was created and these stresses are considered together with the Von Mises yield criterion.

Implementation and solution

The described model was implemented in a FE mesh generator called RISERTOOLS, which generates FE meshes to be analyzed in ANSYS® program.

Considering the available elements in ANSYS® and the proposed model, the following elements were used: SHELL181 (non-linear shell element) is employed to model the inner carcass, the pressure armor and the polymeric layers of the riser; BEAM188 (non-linear beam element) is used to represent the wires of the tensile armors; and CONTA174 / TARGE170 are used to simulate the contact between the layers of the riser.

In order to solve the set of simultaneous equations generated by the finite element discretization, the sparse solver method was chosen. This method associated to an equation reordering procedure gave accurate results with the least computational effort.

EXPERIMENTAL TESTS

Aiming at studying the extensional-torsional behavior of flexible pipes, the metallic frame presented in Fig. 5 was constructed and installed at the Structures Laboratory of COPPE/UFRJ. This equipment can simulate tension and torsion loads acting simultaneously in pipes with a total length up to 10m.

Figure 5 – View of the metallic frame.

In this work, the structural behavior of a 10m sample of a 4.0” flexible pipe subjected to pure tension was analyzed. The tensile load was cyclically applied to the pipe from zero to a maximum value between 350kN and 450kN and then returned to zero. Three loading-unloading cycles were performed in each test considering two different end conditions:

1. One end free to rotate and the other one clamped.
2. Both ends prevented from rotating with one of them clamped.

Three experiments for each end condition were carried out in order to check for the repeatability.

A general view of the whole experimental apparatus is presented in Fig. 6.

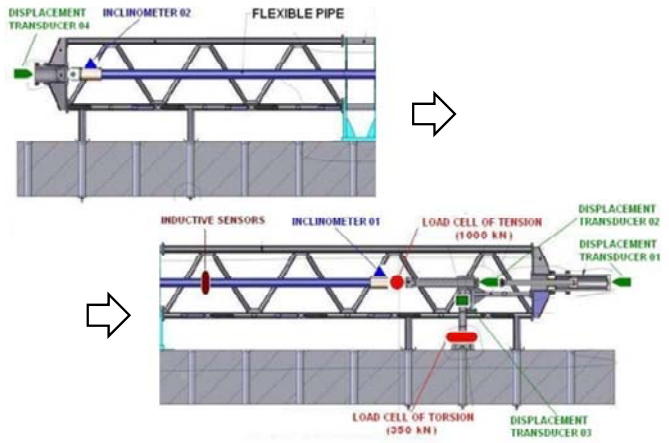

Figure 6 – General view of the experimental apparatus.

The apparatus consisted of two load cells, Fig. 7, devoted to measure the applied tension and the torque reaction of the pipe, when its ends are prevented from rotating.


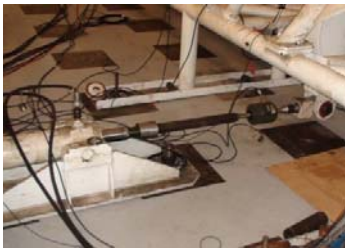

(a) (b)

Figure 7 – Load cells: (a) tension and (b) torsion.

Four displacement transducers were also employed. Three were used to observe the axial displacements of the pipe and one was connected to the torque load cell in order to measure its axial displacement. A detail of the displacement transducer 1 is presented in Fig. 8.

Figure 8 – Detail of the displacement transducer 1.

Moreover, two inclinometers were fixed to metallic plates and linked to the ends of the flexible pipe by magnetic bases, as pointed out in Fig. 9. These inclinometers measured the axial rotation of the pipe.

(a) (b)

Figure 9 – Inclinometers (a) 01 and (b) 02

Finally, six inductive sensors were used to measure the radial variation of the pipe, as shown in Fig. 10. These sensors provide high precision, non-contact position measurement by varying its electrical output in proportion to the position of a metal target within its working range (2.0 – 8.0 mm).

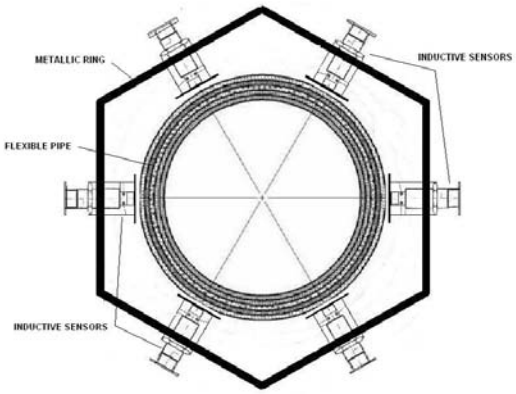

Figure 10 – Inductive sensors.

CASE STUDY

Table 1 presents the main characteristics of the studied 4,0" flexible pipe (internal diameter equals to 101.6mm).

Table 1 – Characteristics of the 4.0" flexible pipe.

Layer	*Properties*
Inner carcass	thickness = 4.0mm; number of wires = 1 lay angle = +87.6°, Interlocked profile area = 32.0mm^2, moment of inertia = 52.1mm^4
Internal plastic sheath	thickness = 5.0mm
Pressure armor	thickness = 6.2mm; number of wires = 2 lay angle = +87.0°, Z profile area = 54.1mm^2, moment of inertia = 173.4mm^4
Anti-wear tape	thickness = 2.0mm
Inner tensile armor	thickness = 2.0mm; number of wires = 47 lay angle = +35.0°, rectangular profile width = 7.0mm
Outer tensile armor	thickness = 2,0mm; number of wires = 49 lay angle = -35.0°; rectangular profile width = 7.0mm
Fabric tape	thickness = 1.15mm
Outer plastic sheath	thickness = 5.0mm

The inner carcass is constituted of AISI 304 steel with a Young modulus of 193GPa and a Poisson coefficient of 0.3. The material of the pressure and tensile armors has Young modulus of 205GPa and Poisson coefficient of 0.3. The internal plastic sheath is made of PA11 with Young modulus of 345MPa and Poisson coefficient of 0.3, while the outer plastic sheath is also formed by PA11, but with Young modulus of 215MPa and Poisson coefficient of 0.3. Finally, the fabric and anti-wear tapes were assumed to have Young modulus of 350MPa and Poisson coefficient of 0.3.

Numerical analyses

A FE model with a total length of 1274mm was constructed. This model has 25922 nodes and 48922 elements leading to 155532 degrees of freedom.

The total length of the model is equivalent to two linear pitches of a wire of the outer tensile armor and is different from the length of the tested pipe in order to reduce computational effort. Since the axial displacement and rotation or the resulting torque of the pipe is directly proportional to the length of the model, this truncated model proved to be valid.

Moreover, this length was found to be, after several mesh trials, enough to guarantee that possible local perturbations caused by the imposed boundary conditions did not affect the response of the pipe as a whole. The extremities of the FE model have coupled displacements in order to simulate the presence of the end-fittings and, therefore, correctly transfer the imposed boundary conditions. Figure 11 illustrates a view of the boundary conditions at an end of the numerical model.

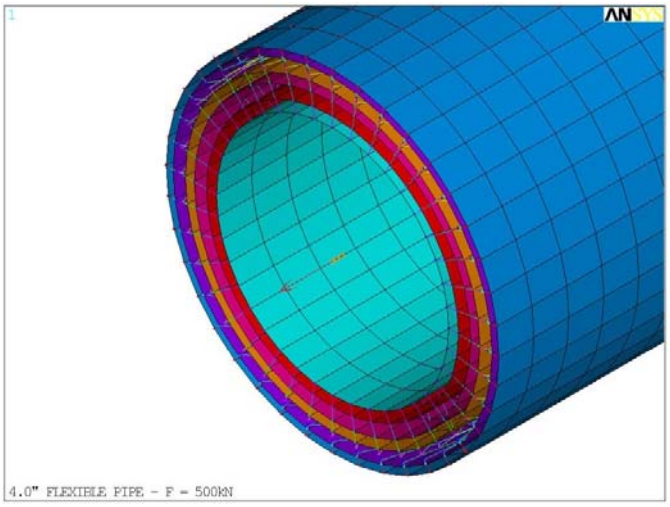

Figure 11 –Boundary conditions at an end of the flexible pipe (axial rotation restrained and imposed axial force).

In order to compare the numerical results to the experimental ones, the same boundary conditions considered in the experimental tests were also assumed here.

Furthermore, a parametric study to evaluate the effect of different friction coefficients between layers was also carried out. For the sake of comparisons, the same friction coefficient was assumed in all interfaces in each analysis. Friction coefficients of 0 (free sliding), 0.05, 0.10, 0.20, 0.40, 0.60 and 1.00 were considered. Moreover, a bonded situation, which corresponds to infinite friction coefficient between layers, was also considered

Numerical results

Figure 12 presents the distribution of the axial displacements obtained in the analysis with free sliding between all layers of the pipe and with ends free to rotate. This distribution is similar to the ones obtained in all other analyses, *i. e.*, the axial displacements are directly proportional to the length of the model.

Tables 2 and 3 present the ratio between the imposed tension, F, and the axial deformation, ε, obtained in each numerical analysis performed. The ratio between the axial rotation, ϕ, or torque, T, and the associated axial deformation and the ratio between the radial displacement, ΔD, and the axial deformation are also presented.

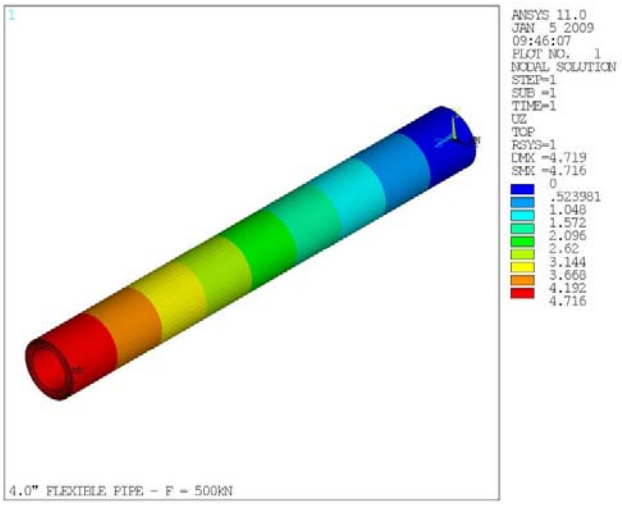

Figure 12 – Axial displacement distribution, in *mm*, along the flexible pipe.

Table 2 – Axial displacements and rotations with free axial rotation at an end of the flexible pipe.

Friction coefficient	F / ε (x10^{2}kNm/m)	ϕ / ε (x10^{2}deg m/m)	$\Delta D / \varepsilon$ (x10^{2}m^2/m)
0.00	1350.990	0.26262	-0.1911
0.05	1351.076	0.26150	-0.1911
0.10	1351.105	0.26061	-0.1911
0.20	1351.191	0.25905	-0.1911
0.40	1351.248	0.25702	-0.1911
0.60	1351.277	0.25493	-0.1911
1.00	1351.334	0.25310	-0.1911
Bonded	1352.195	0.00000	-0.1911

Table 3 – Axial displacements and torque with axial rotation restrained at the ends of the flexible pipe.

Friction coefficient	F / ε (x10^{2}kNm/m)	T / ε (x10^{2}kNm^2/m)	$\Delta D / \varepsilon$ (x10^{2}m^2/m)
0.00	1352.281	2.099	-0.1923
0.05	1352.281	2.099	-0.1923
0.10	1352.281	2.099	-0.1923
0.20	1352.281	2.099	-0.1923
0.40	1352.309	2.099	-0.1923
0.60	1352.309	2.099	-0.1923
1.00	1352.309	2.099	-0.1923
Bonded	1352.309	2.099	-0.1923

Tables 2 and 3 point that the axial stiffness of the pipe is not dependent on the friction between layers. When one of its end is free to rotate, the obtained no friction stiffness is only 0,09% lower than the bonded stiffness and, when its ends are prevented from rotating, this difference is lower than 0.01%. The axial stiffness is also not altered by the restriction of the axial rotation.

Furthermore, the induced axial rotation is quite small and also slightly affected by the friction coefficient, when this value is kept between 0.00 and 1.00. The estimated axial rotation for the no friction case is only 3.8% higher than the one calculated with a friction coefficient of 1.0. However, when the layers of the pipe are fully bonded, the axial rotation is zero. When the ends of the pipe are clamped, the induced torque is not altered by the friction between layers.

The radial constriction of the pipe is also very small and not sensible to the friction between layers. Constant values were found in both analyzed cases and the ones estimated with ends prevented from rotating are slightly higher (0.6%) than the radial displacements calculated with free axial rotation.

Thus, the analyzed flexible pipe is torque balanced since the axial rotations induced by the tensile load is quite small and its axial stiffness is not altered by the axial rotation restriction.

It is now important to observe the displacements predicted for each section of the pipe. Figure 13 presents the axial translations in each layer and cross-section of the pipe when one of its ends is free to rotate and no friction between layers is considered. Figure 14 presents the axial rotations for the same case. In these figures, position 0mm (first cross-section) is the clamped end of the pipe.

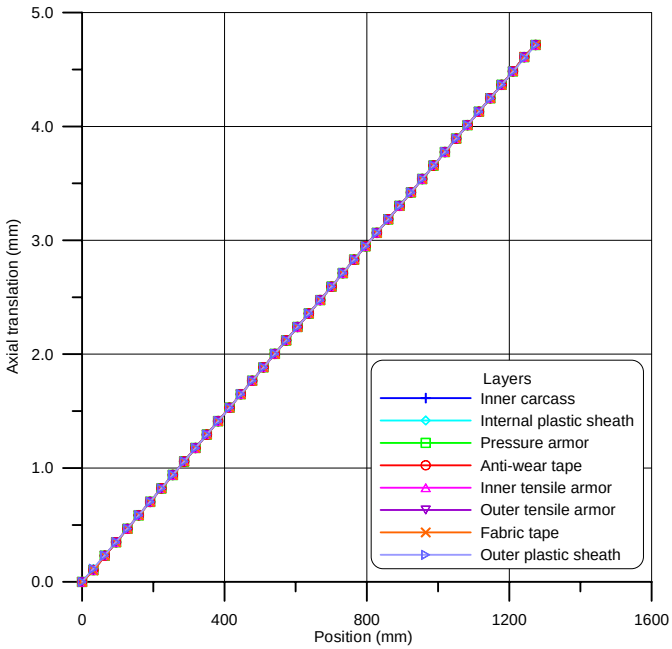

Figure 13 – Axial translations in each layer and cross-section of the pipe: end free to rotate.

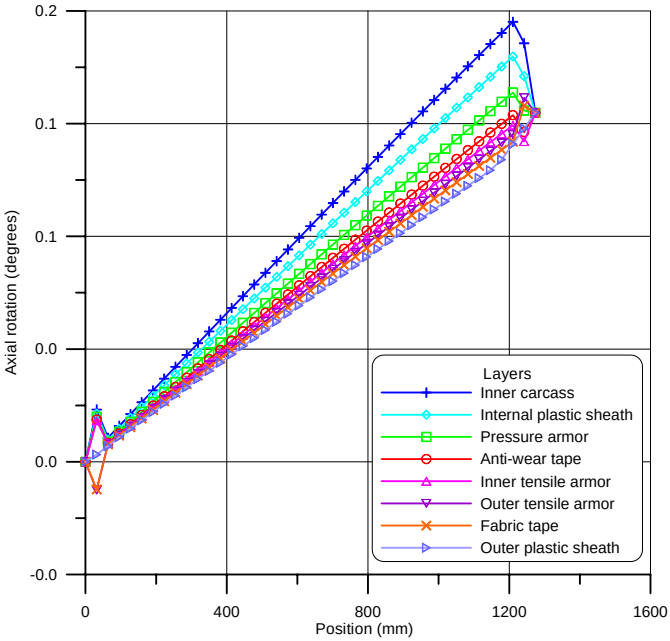

Figure 14 – Axial rotations in each layer and cross-section of the pipe.

Figure 13 shows that the axial translation is the same in each layer and cross-section of the pipe. It varies linearly with respect to the position of the cross-section. Figure 14 presents small regions near the extremities of the model in which the axial rotation is locally affected by the imposed boundary conditions. However, out of these regions, the calculated axial rotations are not the same in all layers of the pipe. Thus, the cross-sections of the pipe remain straight, but the axial rotations in each of its layers are different.

On the other hand, when the ends are prevented from rotating, the axial rotations along the pipe are null and, consequently, the hypothesis of straight section with the same twist in each layer is valid.

A common assumption of analytical models devoted to the axisymmetric analysis of flexible pipes is that axial translations and rotations are the same for all layers of the pipe and in each of its cross-sections. As pointed out previously, this is not confirmed by the FE model when the ends are not prevented from rotating and may affect the prediction of the axisymmetric response of a flexible pipe.

Numerical and experimental comparisons

Figure 15 presents the experimental measures of the flexible pipe axial deformations with respect to the applied tension. In this figure, the end of the pipe is free to twist. Figure 16 shows the same variation, but, in this case, the ends of the pipe are prevented from rotating.

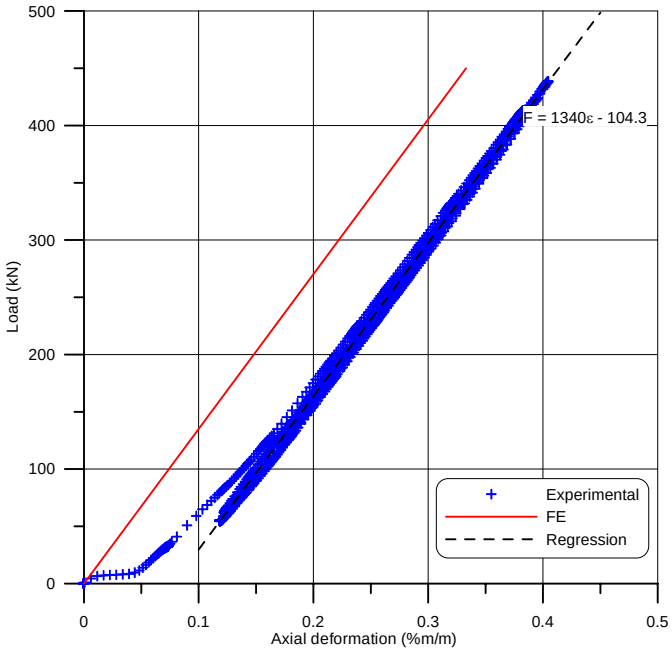

Figure 15 – Axial deformation *vs* applied tension: ends free to rotate.

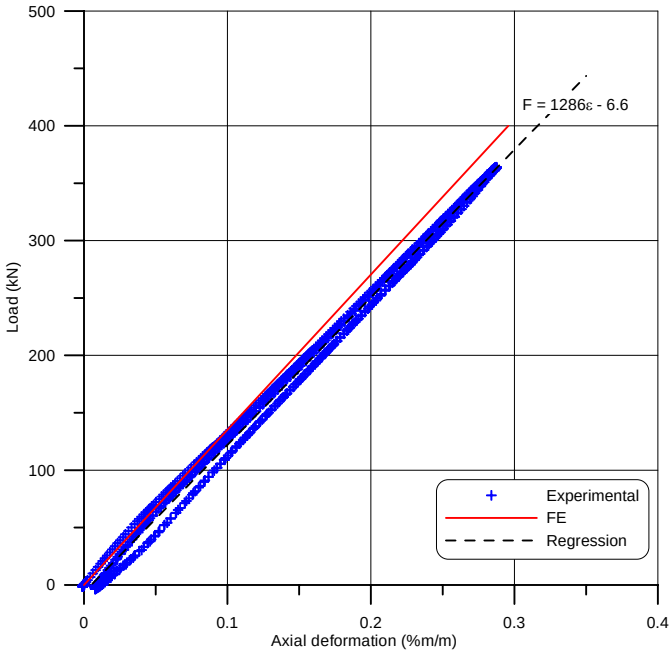

Figure 16 – Axial deformation *vs* applied tension: ends prevented from rotate.

Figure 15 shows, after an initial accommodation caused by initial gaps between the layers of the pipe and the initial catenary configuration due to its self weight , that the axial deformation of the pipe varies linearly with the imposed tension. During the loading or unloading phases, no significant modification in the axial stiffness of the pipe is observed. A linear function was fitted to the experimental points leading to an axial stiffness of 134000kN, which is only 0.8% lower than the value predicted by the FE model when no friction is considered. The FE curve is also plotted in Figure 15.

Figure 16 presents a similar behavior, but no initial accommodation was observed. In these tests, the linear fit indicates an axial stiffness of 128600kNm/m, which is only 4.0% lower than the stiffness estimated in the tests with ends free to rotate and 4.8% lower than the FE axial stiffness.

Hence, it can be concluded that the restriction of the axial rotation did not alter the axial stiffness of the pipe.

Figures 17 and 18 deal with the induced axial rotation and torque in the pipe, respectively. In Fig. 17, besides the experimental points, three more curves are presented. Two bilinear functions were fitted to the experimental points: one for the loading phases and the other to the unloading phases. Moreover, the curve predicted by the FE model with no friction is also plotted. In Fig. 18, three curves are showed with the experimental points: two linear functions were fitted to the experimental points after a 0.18% axial deformation is reached; and the FE curve estimated with no friction between layers.

These figures present a highly nonlinear response. In Fig. 17, the axial rotation of the pipe, after the accommodation phase, grows almost linearly until the load is reversed. When the reversal occurs, the axial rotation initially increases with a small reduction in the axial deformation and then it starts to decrease in a constant rate. However, when an axial deformation of about 0.28%m/m is reached, the ratio between the axial rotation and deformation decreases to a value of about a third of the previous one. When the pipe is reloaded, the initial ratio is almost equal to the low value exhibited in the end of the unloading phase, but, when an axial deformation of about 0.3%m/m is achieved, the relation between the axial rotation and deformation increases to a value three times higher. This type of response was observed in all three loading-unloading cycles.

The experimentally measured axial rotations suggest that some kind of adhesion may exist between the layers of the pipe, as the transition between loading and unloading phases and even the response of the pipe during these phases involves significant changes in the relation between the axial rotation and elongation. The higher values obtained for this ratio is, in average, only 6.8% higher than the FE one (26.262deg m/m) when no friction is considered. This high value is reached when significant tension is acting and, consequently, a possible internal friction in the pipe is overcame. The lower value corresponds to about 35% of the FE one and is observed when low tension is acting, which indicates that this is related to some initial internal friction or adhesion between the layers of the pipe. Some FE simulations were performed in order to obtain this low value and very large values for the friction coefficient between layers (higher than 100) were necessary.

In Fig. 18, the response of the pipe is initially quite mixed. The ratio between the induced torque and the axial deformation increases and decreases in a highly nonlinear way until an axial deformation of about 0.18%m/m is achieved. After that, this ratio is almost constant and the variation of the torque with

respect to the axial deformation is approximately linear. The average experimental value for this ratio (average of the two linear functions) is only 1.7% lower than the FE predicted one ($2.099 kNm^2/m$).

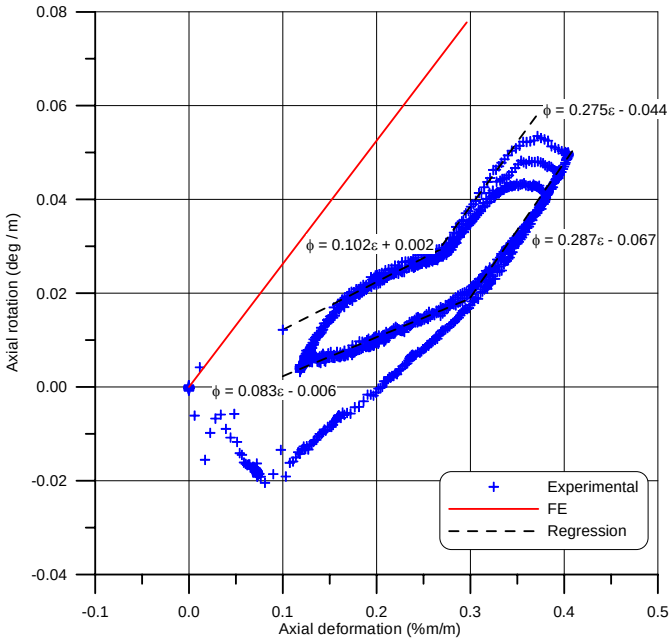

Figure 17 – Axial deformation *vs* Axial rotation: ends free to rotate.

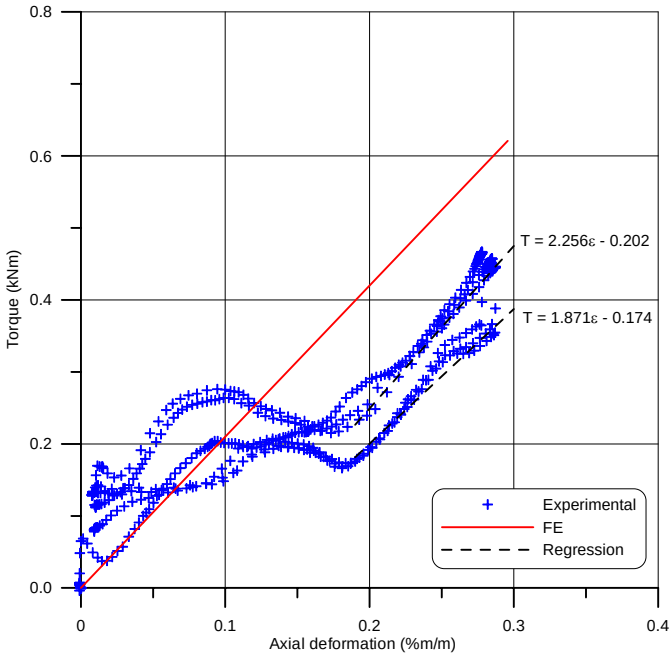

Figure 18 – Axial deformation *vs* torque: ends prevented from rotating.

Figures 19 and 20 illustrate the variation of the radial displacement of the pipe with its axial deformation for the case in which the ends are free to rotate and prevented from rotating, respectively.

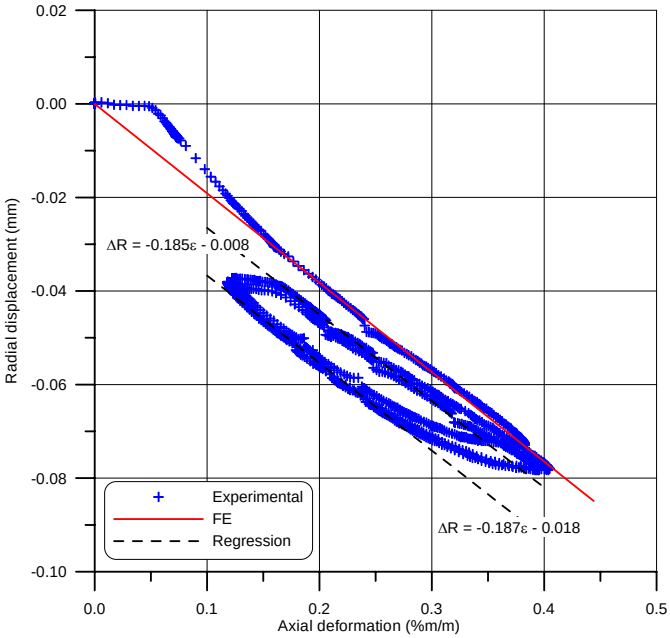

Figure 19 – Axial deformation *vs* radial displacement: ends free to rotate.

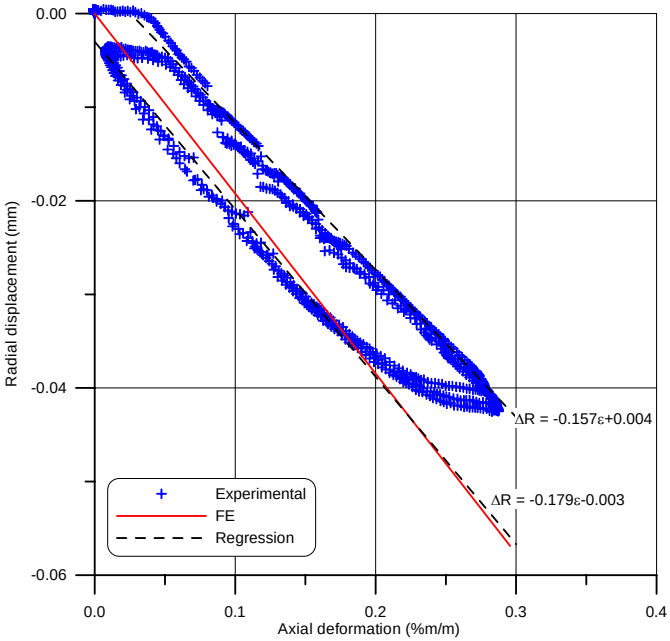

Figure 20 – Axial deformation *vs* radial displacement: ends prevented from rotating.

These figures show the same behavior. There is an initial accommodation of the pipe followed by a linear variation between the axial deformation and the radial constriction. When the load is reversed, an initial accommodation phase

occurs again and, after that, the radial displacement starts to linearly decrease. The linear functions fitted to the experimental measurements presented in Figs. 19 and 20 led to close values for the ratio between the radial displacement and the axial deformation: -18.6m^2/m and -16.8 m^2/m (average). This indicates that the restriction of the axial rotation does not affect the radial displacements in the pipe. These values are about 3.0% (ends free to rotate) and 12.5% (ends prevented from rotating) lower than the FE ones (-19.1m^2/m and -19.2m^2/m, respectively).

Finally, it is important to observe that the nonlinear behavior observed for the axial rotation and torque in the experimental test is not seen in the axial deformation of the pipe. This is also stated by the FE model since the variation of the friction coefficients, as pointed in Tables 3 and 4, did not imply any significant modification in the axial stiffness of the pipe.

CONCLUSIONS

This paper dealt with the coupled extensional-torsional behavior of a 4" flexible pipe. The pipe was subjected to pure tension and two different boundary conditions were considered: ends free and prevented from axially rotating. The response of the pipe was predicted with a proposed three-dimensional nonlinear finite element (FE) model. Some aspects of the obtained results are discussed, such as:

1. The effect of restraining the axial rotation at the extreme sections of the model.
2. The effect of friction or adhesion between the layers of the pipe on the induced axial rotation (or torque), elongation and radial constriction of the pipe.
3. The reduction to simple plane behavior usually assumed by analytical models.

The numerical results predicted that the axial stiffness and the radial displacements of the pipe did not vary with the restriction of the axial rotation at its extremities. Moreover, the model indicated that the amount of friction between the layers of the pipe also did not affect its axial stiffness or radial displacements. The FE model also pointed to very low values for the induced axial rotation or torque at the extremities. Furthermore, the axial rotation was slightly changed when friction coefficients between 0.0 and 1.0 were considered, but decreases to 0 if the layers of the pipe are supposed to be bonded (very high values of friction coefficients). The induced torque also did not vary with the considered friction coefficients.

An important aspect verified in the numerical analysis was that the sections of the pipe elongates equally, but the axial rotations are different in each layer. Thus, the assumption that all layers are subjected to the same axial rotation is not valid.

The experimental tests pointed to a nonlinear response of the pipe to the imposed tension. This nonlinear behavior is caused mainly by:

- The initial configuration of the pipe, which usually presents initial gaps between its layers and a catenary shape due to its self-weight.
- Friction between the layers.

The initial configuration of the pipe provokes an accommodation phase when low tensile loads are being applied (large axial deformations with low tension), while friction significantly modifies the induced axial rotation and torque in the pipe, but seems to not alter its axial stiffness or radial constriction.

When compared to the experimental measurements, the predicted FE results agreed quite well. The measured axial stiffness were between 0.8% (ends free to rotate) and 4.8% (ends prevented from rotating) lower than the FE calculated ones. Moreover, the measured ratio between the radial displacement of the pipe and its axial deformation was between 3.0% (ends free to rotate) and 12.5% (ends prevented from rotating).

The no friction ratio between axial rotation and elongation was only 7.3% higher than the measured one for high tensile loads. For low tensile loads, the measured ratio is about a third of this FE one. This low tension ratio was achieved with the FE model when very high friction coefficients were considered and suggests the existence of an initial adhesion between the layers of the pipe.

Analogous to the variation of the axial rotation, the induced torque also initially exhibits a highly nonlinear behavior, but, for high tensile loads, it tends to vary linearly with the axial elongation. Again, for this level of loading, the numerical results agreed quite well with the experimental ones.

To conclude with, it is authors belief that this work contributes to better comprehend the behavior of a flexible pipe under tension and the effect of friction on its response. Besides, it presents a robust three-dimensional FE model to deal with the local mechanical analysis of flexible pipes. The obtained results also encourage the use of this model to analyze other types of axisymmetric loads such as internal and external pressure, torsion and axial compression and possible combinations between them.

ACKNOWLEDGMENTS

The authors wish to acknowledge the invaluable support from ANP (National Petroleum Agency) to their researches. The experiments described in this paper were only possible due to research cooperation with the Federal University of Rio de Janeiro.

REFERENCES

[1] Ferét, J. J., and Bournazel, C. L., 1987, "Calculation of Stresses and Slip in Structural Layers of Unbonded Flexible Pipes," Journal of Offshore and Mechanic Arctic Engineering, 109, pp. 263-9.

[2] Witz, J. A., and Tan, Z., 1992, "On the Axial-Torsional Behaviour of Flexible Pipes, Umbilicals and Marine Cables," Marine Structures, 5, pp. 205-27.

[3] Custódio, A. B., and Vaz, M. A., 2002, “A Nonlinear Formulation for the Axisymmetric Response of Umbilical Cables and Flexible Pipes,” Applied Ocean Research, 24, pp. 21-9.
[4] Saevik, S., and Bruaseth, S., 2005, “Theoretical and experimental studies of the axisymmetric behaviour of complex umbilical cross-sections,” Applied Ocean Research, 27, pp. 97-106.
[5] Ribeiro, E. J. B., Sousa, J. R. M., Ellwanger, G. B., and Lima, E. C. P., 2003, “On the Tension-Compression Behaviour of Flexible Risers,” Proceedings of the 13th International Offshore and Polar Engineering Conference, pp. 105-112, Honolulu.
[6] Cruz, F. T. L., 1996, “Structural Analysis of Flexible Pipes through the Finite Element Method,” M.Sc. dissertation, EPUSP, São Paulo, Brazil. (In Portuguese).
[7] Sousa, J. R. M., 1999, “Numerical Analisys of Flexible Risers,” M.Sc. dissertation, COPPE, Federal University of Rio de Janeiro, Rio de Janeiro, Brazil. (In Portuguese).
[8] Bahtui, A., Bahai, H., and Alfano, G., 2008, “A Finite Element Analysis of Unbonded Flexible Risers under Axial Tension,” Proceedings of the ASME 27th OMAE, 57627, Estoril.
[9] Witz, J. A., 1996, “A Case Study in the Cross-Section Analysis of Flexible Risers,” Marine Structures, 9, pp. 885-904.
[10] Ramos Jr., R., Martins, C. A., Pesce, C. P., and Roveri, F. E., 2008, “A Case Study on the Axial-Torsional Behavior of Flexible Risers,” Proceedings of the ASME 27th OMAE, 57514, Estoril.
[11] Ramos Jr, R. and Pesce, C.P., 2004, “A Consistent Analytical Model to Predict the Structural Behavior of FlexibleRisers Subjected to Combined Loads”, Journal of Offshore and Mechanic Arctic Engineering, 126, pp.141-146.
[12] Hobbs, R. E., and Raoof, M., 1982, “Interwire Slippage and Fatigue Prediction in Stranded Cables for TLP Tether,” Proceedings of Behaviour of Offshore Structures (BOSS), 2, pp. 77-99.
[13] Raoof , M., and Hobbs, R. E., 1984, “Analysis of Multilayered Structural Strands,” Journal of Engineering Mechanics Division – ASCE, 114, pp. 1166-82.
[14] Kraincanic, I., 1995, “Analysis of the Coupled Axial/Torsional Behaviour of Spiral Strands, Wire Ropes, and Locked Coil Cables,” B.Sc. dissertation, School of Architecture and Civil Engineering, South Bank University, London.
[15] Timoshenko, S. P., and Woinowsky-Krieger, S., 1959, Theory of Plates and Shells, 2nd edition, McGraw-Hill Kogakusha, Tokyo.
[16] Souza, A. P. F., 2002, “Flexible Pipe’s Collapse under External Pressure,” D.Sc. thesis, COPPE, Federal University of Rio de Janeiro, Rio de Janeiro, Brazil. (In Portuguese).
[17] Belytschko, T., and Neal, M. O., 1991, “Contact-Impact by the Pinball Algorithm with Penalty and Lagrangean Methods,” International Journal of Numerical Methods in Engineering, 31, pp. 547-72.
[18] Belytschko, T., Liu, and W. K., Moran, B., 2000, Nonlinear Finite Elements for Continua and Structures, John Wiley & Sons Ltd, England.
[19] Benson, D. J., and Hallquist, J. O., 1990, “A Single Contact Algorithm for the Postbuckling Analysis of Shell Structures,” Computer Methods in Applied Mechanics and Engineering, 78, pp. 141-63.
[20] Besseling, J. F., 1958, “A Theory of Elastic, Plastic and Creep Deformations of an Initially Isotropic Material Showing Anisotropic Strain-Hardening Creep Recovery and Secondary Creep,” Journal of Applied Mechanics, pp. 529-36.